Progress In Electromagnetics Research Letters, Vol. 41, 135–148, 2013

MEMS COMPATIBLE SEVER FOR 220 GHz ULTRA WIDE BAND TWTA: DESIGN AND PARTICLE-IN-CELL ANALYSIS

Anisullah Baig*, Larry R. Barnett, Diana Gamzina, and Neville C. Luhmann, Jr.

Department of Electrical and Computer Engineering, University of California, Davis, CA 95616, USA

Abstract—We report a MEMS (micro-electro-mechanical systems) compatible distributed loss type sever design for the 220 GHz double vane half period staggered traveling-wave tube amplifier (TWTA) [1]. The cold test simulations for a full TWT model including input/output couplers and broadband tapered vane transitions incorporating the sever, predicted a return loss (S_{11}) of < -10 dB in the pass band (205 GHz–275 GHz) while an insertion loss/isolation (S_{21}) of ~ -27 dB. The return loss of the TWT circuit did not degrade by the inclusion of the sever (< -10 dB) while still maintaining a good isolation (S_{21}) for the RF signal. Particle-In-Cell (PIC) simulation analysis for the full 220 GHz TWT circuit (a) without sever and (b) with sever was conducted. With the inclusion of the sever, the TWTA showed generally a stabilized output response for all cases. The maximum power from the long sever case was ~ 25 W for $P_{in} \sim 50$ mW and the gain was ~ 27 dB. The reverse power was decreased to ~ 30 mW. For the short sever, the PIC results were even better with a maximum output power of ~ 62 W and a gain of ~ 30.92 dB with a reduced reverse power of ~ 5 mW for an input power of 50 mW at 220 GHz. The FFT spectrum of the RF signal at the output port also showed a spectrally pure waveform at 220 GHz.

Received 20 March 2013, Accepted 10 May 2013, Scheduled 19 July 2013

* Corresponding author: Anisullah Baig (abaig@ucdavis.edu).

1. INTRODUCTION

In the last decade, there has been considerable work aimed at the realization of compact and mobile sources in the THz regime of the electromagnetic spectrum (0.1–1 THz) [2]. It is well established that this mmwave — THz range of frequencies has unique features including its non-ionizing radiation characteristics, ability to pass through packaging materials and clothing, and strong signal-to-noise ratio in the presence of fog and water content. This leads to a variety of potential applications [3] that include non-invasive detection of contraband items, industrial quality control, plasma and medical imaging, all-weather visibility, and advanced telecommunication system applications.

VED (Vacuum Electron Device) technology remains at the top for providing high power [4] at almost all frequency ranges of available microwave/millimeter devices. The sheet beam topology in micro-vacuum electron devices provides further benefit through the use of planar slow wave structures where the beam tunnel is squashed in one dimension and stretched in other. This makes possible high current transmission at moderate magnetic fields in addition to the benefit of the compatibility of sheet electron beam type SWS planar structures with MEMS fabrication schemes [4].

VEDs with reasonably high power device (> 10 W) at millimeter wave — THz frequencies, demands high conversion efficiency. For a typical TWTA, the reflected wave in the slow wave structure (SWS) from the impedance mismatch at the input and output couplers could cause instability and feedback oscillations that affects the efficiency of the tube. To counter this instability, typically the TWT structure is electrically disconnected or severed in the middle [5, 6]. The amplitude of the forward growing wave drops at the sever location; however, the wave starts growing again after the sever, attributed to the modulation carried forward by the electron bunching. The challenge for a sever design is to attenuate the forward wave over a wide range of frequencies and at the same time not letting the reflections to build up in the circuit. This needs an efficient impedance matching in the sever structure over a wide bandwidth [7, 8]. Moreover, the classic sever is comprised of two separate ports loaded with loss material that attenuates the forward going wave and the reflected wave. However, at THz frequencies where the familiar $P \sim 1/f^2$ scaling fails and μVEDs (micro-scale Vacuum Electron Devices) struggle to maintain reasonable efficiency and permanent magnet focusing particularly for the case of a sheet electron beam TWTA, there is a need for an appropriate distributed loss type sever that does not need separate couplers in

the middle of TWTA [9–11] and compatible with advanced fabrication techniques.

In the present work, a novel distributed sever for a planar SWS structure was designed and analyzed that not only is compatible with MEMS fabrication schemes [12] and excludes the need for the additional ports in the middle of structure, it also provides wide-band impedance matching by a tapered vane design. By not using separate ports in the middle, the length of the TWTA structure is reduced, which is promising for employing PPM (periodic permanent magnet) design [13] for a truly compact and light weight TWT package. This paper report the associated design efforts using cold test simulation and extensive Particle-In-Cell simulations.

2. 220 GHz ULTRA WIDEBAND TWTA

Figure 1(a) shows the half-period staggered double-vane array based TWTA circuit [1, 14]. The beam parameters are 20 kV, and 250 mA with a sheet electron beam area of $\sim 0.055\,\text{mm}^2$ with a beam tunnel width of $\sim 770\,\mu\text{m}$ and height $\sim 150\,\mu\text{m}$. For a high current density cathode loading of $\sim 40\,\text{A/cm}^2$, the current density in the tunnel area

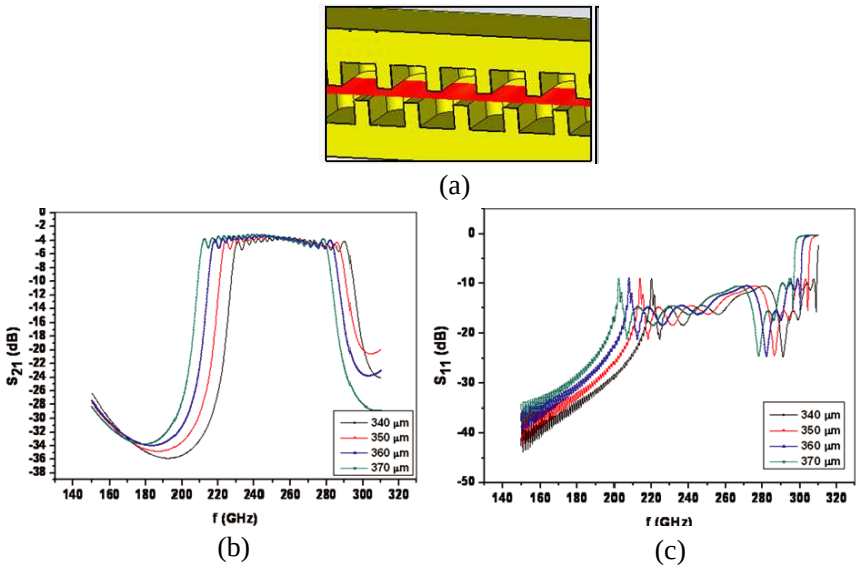

Figure 1. 220 GHz TWTA cold test simulation for different height of the slow wave structure. (a) Sheet beam TWT circuit diagram. (b) Transmission/reflection analysis.

is $\sim 450\,\mathrm{A/cm^2}$ with a compression ratio of $\sim 85\%$ in the top-to-bottom and $\sim 12\%$ compression right-to-left of the beam for the formation of an elliptical beam. The PIC simulations suggested an output power $> 50\,\mathrm{W}$ for a hot bandwidth of $> 60\,\mathrm{GHz}$ for an operating frequency of 220 GHz [15]. This UCD design gives wideband synchronism and the planar structure is compatible with MEMS fabrication schemes and Nano-CNC milling technology. The cold test bandwidth exceeds $\sim 70\,\mathrm{GHz}$ as shown in Figures 1(b), (c) for different heights of one circuit half of the TWTA.

3. MEMS COMPATIBLE WIDEBAND DISTRIBUTED SEVER ($\sim 12\,\mathrm{mm}$) FOR 220 GHz SHEET BEAM TWT AMPLIFIER

As mentioned earlier, for a wideband high power TWT amplifier it is crucial to have a sever that attenuates the forward going wave and does not result in reflections. To accomplish this task while accounting for fabrication challenges, a tapered loss material approach was employed in the cavities of the SBTWT (Sheet beam traveling wave tube amplifier). The idea is to have a wideband impedance matching through tapering and an optimized placement of the sever in the TWT structure for maximizing the RF gain. Figure 2(a) shows the annealed OFHC (Oxygen Free high Conductivity Copper) casing that houses the TWT. The thickness of the loss layer (Si/SiC) [16, 17] is linearly increased in the cavities to a maximum thickness of $\cong 270\,\mu\mathrm{m}$ (i.e., the cavity depth) and decreased back again. The loss material was inserted in the cavities of the TWT with varying depth up to a distance of $\sim 12\,\mathrm{mm}$ almost $\sim 1/3$ of the total length of the slow wave structure. The loss material (Si/SiC) [16, 17] is shown in grey color in the figure.

Figure 2(b) shows that the reflection (S_{11}) in the circuit is down to $\sim -10\,\mathrm{dB}$ in the passband (~ 205–$280\,\mathrm{GHz}$). It is to be noted that the S_{11} value in the circuit without sever also shows the similar trend in reflections ($\sim -10\,\mathrm{dB}$ or better). However, for this sever, a peak around 247 GHz was noted which could be attributed to a trapped mode or mode conversion issues. The best isolation (S_{21}) achieved was $\sim -30\,\mathrm{dB}$ or better by varying the conductivity (engineered) of loss material from $10\,\mathrm{S/m}$ to $1000\,\mathrm{S/m}$. The RF loss in sever at high powers could be an issue particularly for a long pulse/CW operation, but our plan is to operate the TWTA in short pulse/low duty mode for a proof-of-principle test. Before discussing the even shorter and better performance $\sim 4\,\mathrm{mm}$ sever, it is useful to first discuss the Particle-In-Cell results for the 12 mm sever design.

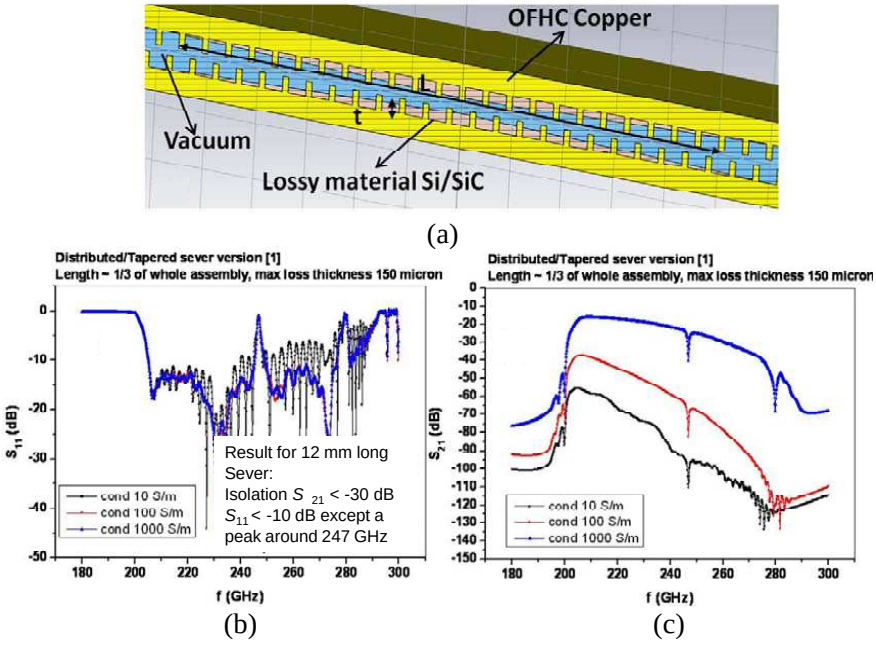

Figure 2. (a) Distributed tapered sever of length $\sim 12\,\text{mm}$. (b) Isolation, S_{21} versus frequency for different conductivities $10\,\text{S/m}$ to $1000\,\text{S/m}$.

4. PARTICLE-IN-CELL (PIC) ANALYSIS OF LONG SEVER $\sim 12\,\text{mm}$ AT DIFFERENT CONDUCTIVITIES

For PIC/Hot test simulation analysis, the TWTA circuit that incorporates the input/output couplers is employed to keep the electron beam and electromagnetic wave separate in the incoming channel. Figures 3(a)–(d) show the PIC results and the PIC simulation model for an $\sim 12\,\text{mm}$ long sever. The power output versus conductivity plot shows that the output power increases for conductivities $> 10\,\text{S/m}$ and reaches to about $\sim 25\,\text{W}$ at a sever conductivity of $\sim 1000\,\text{S/m}$, while the reflected power contained to $\sim 30\,\text{mW}$ at this conductivity. Figure 3(c) shows that the gain that has a minimum at around $10\,\text{S/m}$. It is clear that for conductivities $> 10\,\text{S/m}$, the gain increases but the reflections build up is small as compared to the conductivities $< 10\,\text{S/m}$. At the same time, it has to be considered that a particular conductivity value should be practically achievable [16, 17]. In this regard, a conductivity of $1000\,\text{S/m}$ was

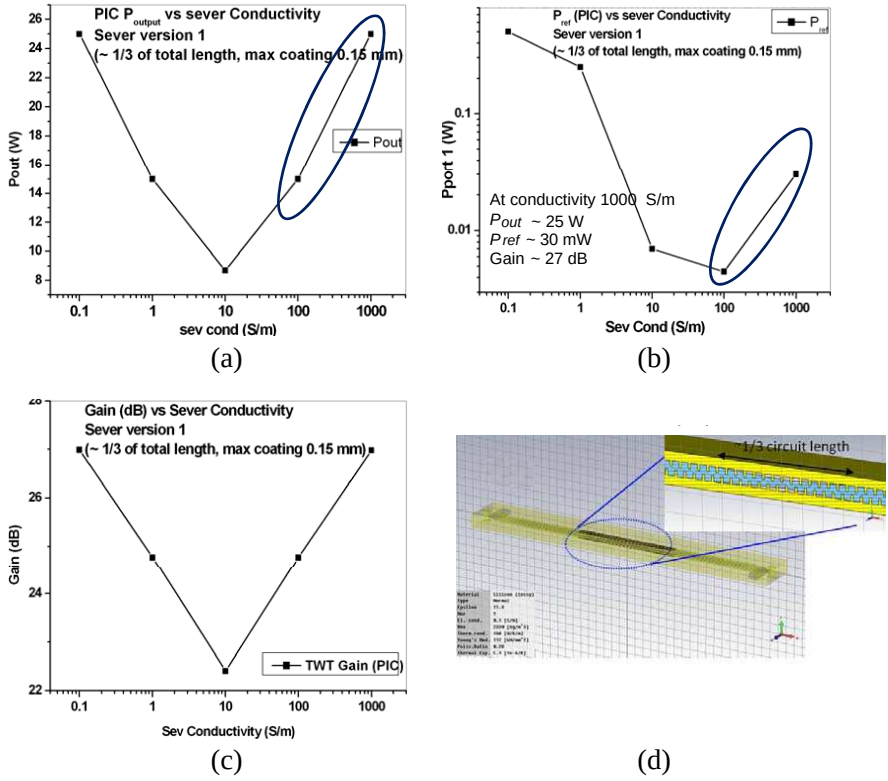

Figure 3. Sever optimization in hot test simulation analysis. (a) Output power versus conductivity of loss material. (b) Reflected power at input port at different conductivities. (c) Gain (dB) versus sever conductivity. (d) TWTA model incorporating broadband couplers and sever in the middle of the circuit.

chosen for this design that predicted a gain of $\sim$27 dB at 220 GHz for the model that incorporates the 12 mm sever.

Figure 4 shows the comparison of output performance of the tube (a) with sever, and (b) without sever. For the TWT model without sever, an instability in the tube is observed on the reflective time scale of $\sim$ 1 nsec. The PIC simulation with the inclusion of the long sever, however, appears to stabilize the tube. Although for the long sever design, there is further room for improvement by optimizing the position of the sever [18] in the beam tunnel, from fabrication point of view, it was decided to shorten the sever to $\sim$1/10 of the SWS structure length. However, the long sever studies did establish that the inclusion

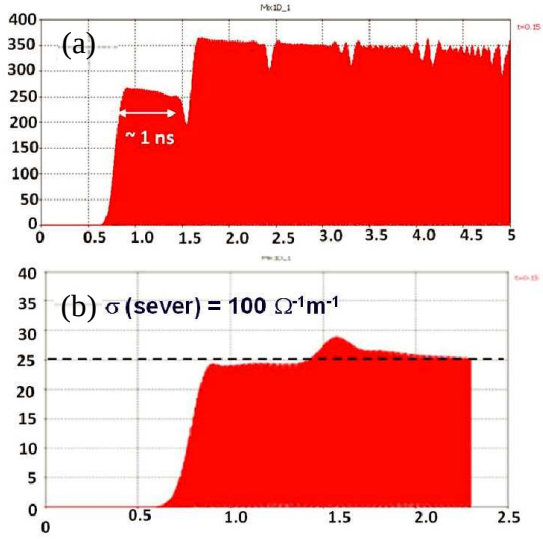

Figure 4. (a) The paticle-in-cell (PIC) response of the TWTA circuit with (a) no sever, (b) with long sever ∼1/3 length of TWTA (∼12 mm).

of the sever does not degrade the performance of the tube significantly and rather helps stabilizing the tube and minimizing reflections at the same time while maintaining gain at a reasonable level.

5. MEMS COMPATIBLE WIDEBAND DISTRIBUTED SEVER (∼ 4 mm) FOR 220 GHz SHEET BEAM TWT AMPLIFIER

It is useful to constrain the sever design to be compatible to the MEMS fabrication processes and techniques available in a typical class 100 clean room. From this point of view, extensive simulations were conducted to reduce the length of the sever to only comprise eight to nine vanes. This also provides a benefit if the loss material shims or in powder form is inserted in the cavities of the slow wave circuit to the required depth. It has also been discussed that one could employ a mask with an opening only on top of the cavities where the loss material is required. This will ensure that loss material is deposited into the cavities and doesn't migrate to the beam tunnel area. This is important for practical TWT amplifier operation as any impurity present in the beam tunnel could poison the high current density cathode. Another aspect that should be considered is the out gassing of the material.

For the convenience in the MEMS fabrication and process, a relatively short sever $\sim 1/10$ of the slow wave structure length was also designed. Figure 5(a) shows the cold test (S-matrix) simulation model. Figures 5(b), (c) show the cold test simulation results. The isolation (attenuation level of the forward traveling electromagnetic wave) achieved was $\sim -27.6\,\text{dB}$ while keeping the reflections low to about $\sim -10\,\text{dB}$. It is necessary to analyze the placement of the sever in the beam tunnel. The position should be such that the beam-wave interaction has already taken place which is indicated through observation of small signal RF gain. This is due to the fact that the sever electrically disconnects the RF channel while the modulation information is carried through the electron bunches which necessitates electron beam and RF interaction before the circuit is subjected to loss material/sever. On the other hand, the placement of the sever should not be very far as compared to the electron emission location which could result in a significant reduction of gain at the sever which could not be compensated for, in the rest of the available tube length.

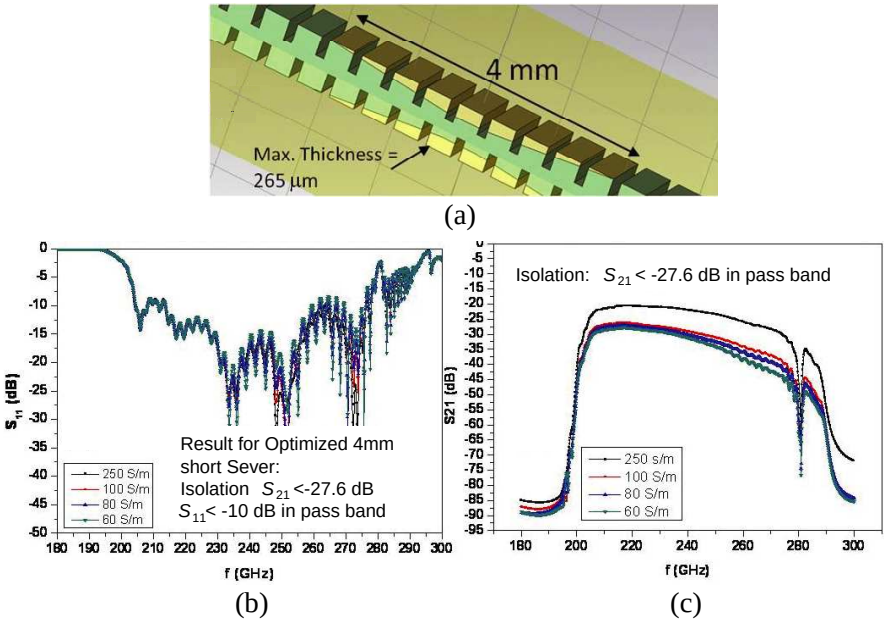

Figure 5. Distributed tapered sever of $\sim 4\,\text{mm}$ length. (a) TWTA simulation model incorporating a sever. (b) Reflections in the TWTA circuit with sever for varying conductivities. (c) Isolation level achieved by using the 4 mm sever for different conductivities.

6. PARTICLE-IN-CELL (PIC) ANALYSIS OF SHORT SEVER ~ 4 MM AND OPTIMIZATION

PIC/hot test simulation was conducted for the 220 GHz TWT model incorporating the 4 mm long sever, to optimize the location for maximizing the gain and minimizing the reflections. Figure 6(a) shows the output power versus sever position in the TWT slow wave structure. At the optimum location, the gain is maximum and is $\sim$31 dB. Figure 6(b) shows that the reflected power minimum ($\sim$5 mW) occurs at the same optimum location. This is further described in Figures 7(a)–(d). The output power of $\sim$60 W is observed with a gain of $\sim$31 dB at 220 GHz, for an input peak drive of 50 mW. The reflected power remains at a reasonable level ($\sim$ 5 mW). This is crucial as the reflected power could damage the RF driver and an isolator could add as much as $\sim$ 2 to 3 dB loss at the input section of the tube. Hence, this sever design could obviate the need for an isolator and increase the effective power at the input section which is important since power is at a premium at such high frequency. Figure 7(d) shows the FFT amplitude of the RF signal at the output port versus frequency. It is observed that the peak occurs at the excitation frequency (i.e., 220 GHz) and no side bands or presence of parasitic oscillations are observed.

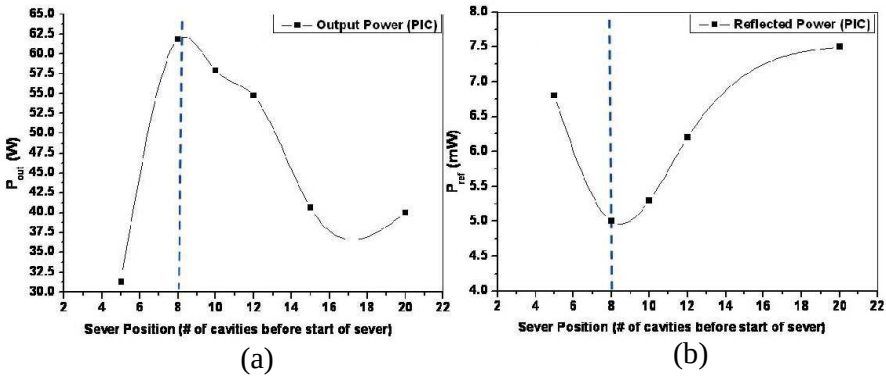

Figure 6. (a) 4 mm sever position optimization in hot test simulation of entire TWTA model. (a) Output power versus sever position. (b) Reflected power versus sever position.

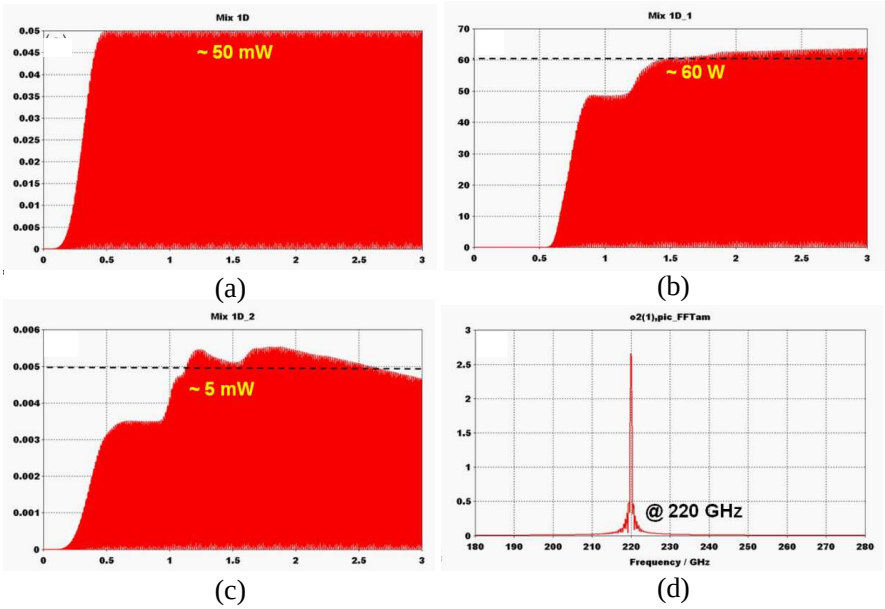

Figure 7. Beam-wave interaction analysis for the TWTA output performance employing 4 mm sever. (a) Input drive of 50 mW. (b) Output power ∼60 W at 220 GHz. (c) Reflected power reduced to ∼5 mW. (d) FFT amplitude of the output signal.

7. SEVER EFFECT ON THE RF ELECTRIC FIELD AND ELECTRON BEAM MODULATION

To demonstrate the effect of electromagnetic field suppression in the sever area and the electron beam that carries the interaction information forward, PIC simulation results are given in Figure 8 for the optimized 4 mm long sever. Figure 8(a) shows that the electromagnetic wave enters the RF channel and travels toward the beam tunnel while the amplitude toward the electron emission side is very low due to the design of the coupler which consists of an RF choke at the electron gun side. Over the first few periods of the slow wave structure, the beam-wave interaction results in a reasonable wave amplification/gain; however, the optimized sever efficiently suppresses this forward growing wave (shown in red circle) and at the same time reduces reflections. Further down the beam tunnel, the RF amplification is clearly shown to grow back again and maximizes in the output coupler area. Figure 8(b) shows that while the sever attenuates the electromagnetic wave, the electron beam carries forward the beam-

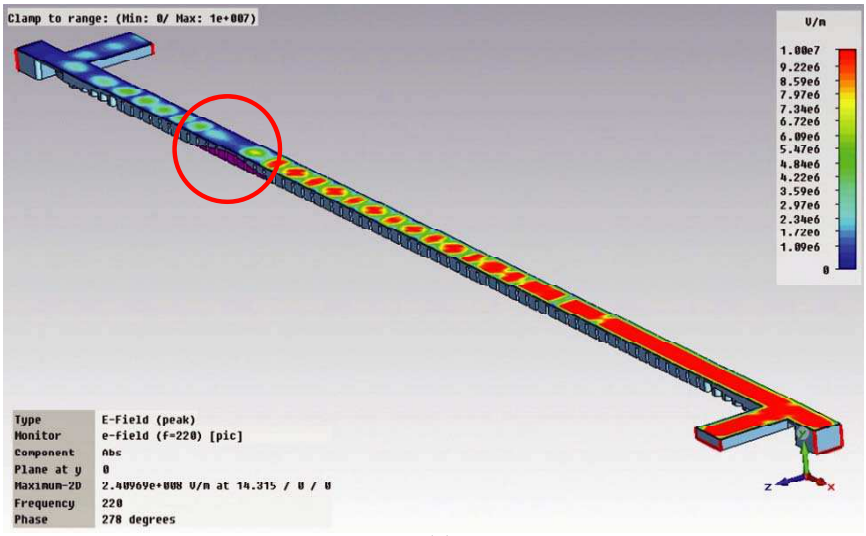

(a)

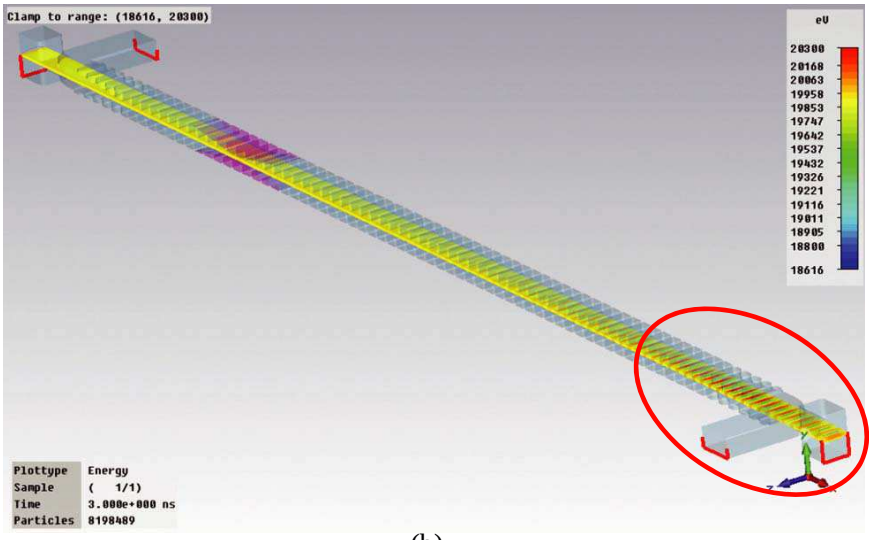

(b)

Figure 8. 220 GHz Traveling Wave Tube Amplifier PIC Model with coupler and sever. (a) E-field amplitude in the sever area and growing wave beam-wave interaction. (b) Electron beam bunching illustrated in the vicinity of output coupler.

wave interaction and beam bunching have been illustrated by a red circle near the output coupler.

8. CONCLUSION

The MEMS compatible distributed sever design using Si/SiC was analyzed for the full model of the 220 GHz double-vane half period staggered TWTA. Two lengths for the distributed tapered sever were considered (a) long sever ~ 12 mm; and (b) short sever ~ 4 mm, to elucidate the effect of length while performing parameter sweeps on thickness and sever conductivity. Cold test simulation and optimization for the 12 mm long sever (case a) suggested a return loss $S_{11} < -10$ dB in the pass band (205 GHz–275 GHz) with an isolation of $S_{21} < -50$ dB except for a peak around 247 GHz. For the 4 mm short sever (case b), the return loss S_{11} was < -10 dB while isolation of $S_{21} \sim -27.6$ dB was achieved in the pass band. As the return loss S_{11} of the TWT circuit without sever is ~ -10 dB, this suggests that the tapered sever design did not deteriorate the S_{11} value while still providing a good isolation for the RF signal.

The output performance of the 220 GHz sheet beam TWTA was analyzed using PIC simulations which were conducted for (a) long server ~ 12 mm; and (b) short sever ~ 4 mm. With the optimization of conductivity, for case (a) a maximum gain of ~ 27 dB was achieved for a peak input power of 50 mW. At the same time, the reflected power was reduced to ~ 30 mW which was quite promising. For case (b), further improvement in terms of compatibility with the MEMS fabrication process (LIGA/DRIE/Nano CNC Milling) with a reduction of the sever size to only ~ 4 mm ($\sim 1/10$ of the length of TWTA) was obtained. The sever position was also optimized to maximize the gain while keeping the reflections low. The maximum gain achieved was ~ 31 dB with an output power of > 60 W and reflected power reduced to ~ 5 mW. Furthermore, the incorporation of the sever in the TWTA also showed stabilization of the output signal.

In conclusion, the S-parameter computations and PIC/hot test analysis for the 220 GHz TWT with the sever showed a promising sever design that could satisfy the TWT design gain bandwidth product goal of ~ 1000 W-GHz with an enhanced stability to the system. Another significant benefit of this type of sever is that it is integrated into the MEMS compatible design of the SWS planar structure and conserves the real estate. The classical sever design typically needs additional sever ports, matching elements, and loss material to attenuate the RF outside the beam tunnel area. Not only does this extend the TWT length, it also makes the magnetostatic design challenging. Hence, for

the sheet electron beam millimeter wave to THz VED regime, where magnet focusing is among the major challenges, this sever design could be a very useful tool to stabilize the tube without suffering from length reduction or magnet focusing problems.

ACKNOWLEDGMENT

This work is supported by the HiFIVE (High Frequency Integrated Vacuum Electronics) program of DARPA (Defense Advanced Research Projects Agency), Grant No. G8U543366), though a subcontract with Teledyne Scientific.

REFERENCES

1. Shin, Y.-M., L. R. Barnett, and N. C. Luhmann, Jr., "Strongly confined plasmonic wave propagation through an ultrawideband staggered double grating waveguide," *Applied Physics Letters*, Vol. 93, 221504-3, 2008.
2. Tonouchi, M., "Cutting-edge terahertz technology," *Nat. Photon.*, Vol. 1, 97–105, 2007.
3. Appleby, R. and H. B. Wallace, "Standoff detection of weapons and contraband in the 100 GHz to 1 THz Region," *IEEE Transactions on Antennas and Propagation*, Vol. 55, 2944, 2007.
4. Booske, J. H., R. J. Dobbs, C. D. Joye, C. L. Kory, G. R. Neil, G.-S. Park, J. Park, and R. J. Temkin, "Vacuum electronic high power terahertz sources," *IEEE Transactions on Terahertz Science and Technology*, Vol. 1, 54–75, 2011.
5. Barker, R. J., N. C. Luhmann, Jr., J. H. Booske, and G. S. Nusinovich, *Modern Microwave and Millimeter-wave Power Electronics,* IEEE/Wiley, 2005.
6. Gilmour, A. S., *Principles of Traveling Wave Tubes,* Artech House, Norwood, MA, 1994.
7. Sesahdri, R., S. Ghosh, A. Bhansiwal, S. Kamath, and P. K. Jain, "A simple analysis of helical slow-wave structure loaded by dielectric embedded metal segments for wideband traveling-wave tubes," *Progress In Electromagnetics Research B*, Vol. 20, 303–320, 2010.
8. Alaria, M. K., A. Bera, R. K. Sharma, and V. Srivastava, "Design and characterization of helix slow wave structure for Ku-band space TWT," *Progress In Electromagnetics Research C*, Vol. 16, 171–182, 2010.

9. Antonsen, T. M., P. Safier, D. P. Chernin, and B. Levush, "Stability of traveling-wave amplifiers with reflections," *IEEE Transactions on Plasma Science*, Vol. 30, 1089–1107, 2002.
10. Kumar, V., A. Vohra, and V. Srivastava, "Nickel and iron as attenuator materials for helix TWT," *Indian Journal of Radio and Space Physics*, Vol. 36, 345–347, 2007.
11. Dialetis, D., D. Chernin, T. M. Antonsen, Jr., and B. Levush, "Accurate representation of attenuation in helix TWT simulation codes," *IEEE Transactions on Electron Devices*, Vol. 56, 935–944, 2009.
12. Baig, A., D. Gamzina, M. Johnson, C. W. Domier, A. Spear, L. R. Barnett, N. C. Luhmann, and Y.-M. Shin, "Experimental characterization of LIGA fabricated 0.22 THz TWT circuits," *IEEE International Vacuum Electronics Conference (IVEC)*, 275–276, 2011.
13. Baig, A., J.-X. Wang, L. R. Barnett, N. C. Luhmann, and Y.-M. Shin, "Beam transport modeling of PPM focused THz sheet beam TWT circuit," *IEEE International Vacuum Electronics Conference (IVEC)*, 351–352, 2011.
14. Shin, Y.-M., L. R. Barnett, and N. C. Luhmann, "Phase-shifted traveling-wave-tube circuit for ultrawideband high-power submillimeter-wave generation," *IEEE Transactions on Electron Devices*, Vol. 56, 706–712, 2009.
15. Baig, A., D. Gamzina, R. Barchfeld, C. Domier, L. R. Barnett, and N. C. Luhmann, Jr., "0.22 THz wideband sheet electron beam traveling wave tube amplifier: Cold test measurements and beam wave interaction analysis," *Physics of Plasmas*, Vol. 19, 093110-8, 2012.
16. http://www-siliconwafer.com/index.html.
17. Mavinakuli, P., S. Wei, Q. Wang, A. B. Karki, S. Dhage, Z. Wang, D. Young, and Z. Guo., "Polypyrrole/silicon carbide nanocomposites with tunable electrical conductivity," *J. Phys. Chem. C.*, Vol. 114, 3874–3882, 2010.
18. Srivastava, V. and R. G. Carter, "Determination of sever positions in a coupled-cavity TWTs," *IEE Proceedings H — Microwaves, Antennas and Propagation*, Vol. 138, 55–60, 1991.